RSC Advances

PAPER

View Article Online
View Journal | View Issue

Cite this: *RSC Adv.*, 2025, **15**, 36514

CRISPR/Cas13a-mediated interfacial cleaving of hairpin RNA reporter for PEAK1 nucleic acid sensing

Xiwei Zhuang,†[a] Zhihao Duan,†[b] Xue Ge,†[b] Yanling Wang,[b] Yuan Gao,[b] Jianlei Liu,[a] Shaoxiong Zhou,[a] Chijia Zeng,*[a] Feiyun Cui*[bc] and Qin Zhou*[bc]

Received 14th July 2025
Accepted 2nd September 2025

DOI: 10.1039/d5ra05024c

rsc.li/rsc-advances

Dysregulation of PEAK1 (pseudopodium-enriched atypical kinase 1) plays a critical role in various cellular processes, including cell migration, proliferation and survival. Its aberrant expression or activity has been implicated in the pathogenesis of several diseases, particularly cancer. Early detection allows for the development and application of targeted therapies that can inhibit PEAK1 activity, potentially improving treatment outcomes. This study provides a new method for early diagnosis of PEAK1 by utilizing the specific RNA cleavage ability of Cas13a combined with electrochemical sensing technology. CRISPR/Cas13 has *cis* cleavage activity and can specifically recognize and cleave target RNA. Subsequently, its *trans* cleavage activity is activated to non-specifically cleave other single stranded RNAs, resulting in detectable signal changes. In the experiments conducted, high sensitivity for detecting PEAK1 mRNA was achieved by optimizing the interface cleavage of the hairpin reporter probe (ReRNA) molecule. The linear detection range is from 1 pg μL^{-1} to 10 ng μL^{-1}, with a detection limit of 0.45 pg μL^{-1}. In addition, the results showed that the developed biosensor has good repeatability, reproducibility, and stability, which provides a novel method for the early screening of PEAK1.

1. Introduce

Pseudopodium-enriched atypical kinase 1 (PEAK1) is an atypical kinase that plays a broad role in biological processes such as cellular signaling, cytoskeletal remodeling, and cell migration.[1,2] In recent years, research has revealed that PEAK1 is critically involved in various medical diseases, particularly in the initiation, progression, and metastasis of cancer. In colorectal cancer, PEAK1 has been frequently observed to be downregulated, and its expression levels are significantly correlated with tumor size, differentiation status, metastasis, and clinical stage.[2] Studies have also demonstrated that exosomal transfer of circular RNA (circRNA) special AT-rich sequence-binding protein 2 (circSATB2), identified as an oncogene in lung cancer, upregulates PEAK1 by acting as a sponge for miR-330-5p, thereby promoting the malignant progression of lung cancer.[3] Research has demonstrated that PEAK1 significantly enhances the invasiveness and metastatic potential of melanoma cells by activating the JAK/STAT3 signaling pathway.[4,5] Specifically, the overexpression of PEAK1 can trigger the JAK/STAT3 signaling pathway, promoting the growth and spread of melanoma cells. Conversely, inhibiting PEAK1 can effectively hinder these processes.[4] Therefore, the early prediction of PEAK1 as a biomarker for diseases such as cancer holds significant importance in helping to predict tumor aggressiveness, metastatic potential, and disease progression rate.[6] This provides critical evidence for clinical decision-making and optimizes treatment strategies.[7]

In mRNA research, PEAK1 mRNA refers to the messenger RNA that encodes the PEAK1 protein.[8] mRNA serves as the direct template for protein biosynthesis, transferring genetic information from DNA to the ribosome, where it directs the synthesis of proteins. As an intermediate carrier of gene expression, mRNA directly reflects the transcriptional state and functional activity of cells.[9] By detecting mRNA expression levels, it is possible to gain in-depth insights into gene regulatory mechanisms,[10] the molecular basis of disease initiation and progression,[11] as well as cellular responses to changes in internal and external environments. The most classical strategy for mRNA detection is reverse transcription polymerase chain reaction (RT-PCR).[12,13] However, this method cannot avoid false-positive signals, which poses a challenge to the specificity of mRNA detection.[14] Additionally, RT-PCR is costly and requires specialized bioinformatics tools and personnel support.[12] Therefore, there is an urgent need for a new technology to achieve the detection of PEAK1 mRNA.

Recent advances in nanomaterial-based electrochemical biosensors have further expanded the detection capabilities for nucleic acids. For instance, Zhang *et al.*.developed a magnetic

[a]*Department of Laboratory, Medicine and Pathology, Foshan Fosun Chancheng Hospital, Foshan, Guangdong 528000, China*

[b]*School of Basic Medical Sciences, Harbin Medical University, Harbin, 150081, China. E-mail: feiyun@hrbmu.edu.cn; zcjiacy@126.com; zhouqin@hrbmu.edu.cn*

[c]*The Heilongjiang Provincial Joint Laboratory of Basic Medicine and Multiple Organ System Diseases (International Cooperation), Harbin, Heilongjiang, 150086, China*

† Xiwei Zhuang, Zhihao Duan and Xue Ge contributed equally to this work.

Fe_3O_4/α-Fe_2O_3@Au nanocomposite-based sensor for ultrasensitive detection of the TP53 gene, highlighting the role of nanomaterials in enhancing electron transfer efficiency.[15] Similarly, Li *et al.* proposed a dendritic hybridization chain reaction (HCR) amplification strategy on an electrochemical platform for detecting RNA methylation modifications, demonstrating the versatility of nanostructured biosensors in epigenetic analysis.[16] Additionally, Liu *et al.* introduced a size-coded DNA probe-based electrochemical multiplexing approach for mRNA splice variant detection, underscoring the adaptability of nanoscale biosensors for complex biomolecular recognition.[14] These studies collectively emphasize the critical role of nanomaterials in improving sensitivity, specificity, and multiplexing capacity of electrochemical biosensors, which aligns with the design principles of our CRISPR/Cas13a-based platform. The unique advantages of electrochemical methods lie in their speed, cost-effectiveness, and exceptional sensitivity, which often surpass those of traditional diagnostic techniques.[15,17,18]

To enable direct detection of mRNA, we introduced CRISPR–Cas13. Cas13a is an RNA-targeting enzyme that utilizes specific CRISPR RNA (crRNA) to guide the recognition and cleavage of complementary RNA sequences.[19] A unique feature of Cas13a is its ability to enter an "activated" state after cutting the target RNA.[20] In this state, it can non-specifically cleave other single-stranded RNA molecules, a phenomenon known as "collateral cleavage".[21,22] This characteristic has led to the development of various Cas13a-based nucleic acid detection technologies, such as SHERLOCK (Specific High Sensitivity Enzymatic Reporter UnLOCKing) and FIND-IT (Fast Integrated Nuclease Detection in Tandem).[20,23] These technologies leverage the activated state of Cas13a to generate detectable signals, allowing for high sensitivity and rapid detection of specific RNA sequences.[24–26]

In this study, by integrating CRISPR–Cas13 with an electrochemical biosensor, we leverage the strengths of both technologies to achieve highly sensitive, specific, and portable RNA detection. The electrochemical transduction mechanism relies on the modulation of electron transfer efficiency at the electrode interface. Specifically, the hairpin-structured ReRNA reporter is terminally labeled with methylene blue (MB), a redox-active molecule that generates a measurable current signal through differential pulse voltammetry (DPV). Upon Cas13a activation, the collateral cleavage of ReRNA results in the detachment of MB from the electrode surface, leading to a quantifiable decrease in the redox current. This signal-off mechanism is highly sensitive to the conformational changes of surface-immobilized RNA probes, as demonstrated by the significant signal enhancement observed with hairpin-structured reporters compared to linear RNA analogs (Fig. 3A and B). Furthermore, the incorporation of gold nanoparticles (AuNPs) *via* electrodeposition increases the effective surface area for probe immobilization, thereby amplifying the electrochemical response. When the target mRNA is present, the Cas13–crRNA complex binds to and cleaves the target RNA, simultaneously activating the nonspecific cleavage activity of Cas13. This nonspecific cleavage further degrades the reporter RNA immobilized on the surface of the electrochemical biosensor, thereby altering the electrochemical signal at the electrode interface. By measuring changes in current, quantitative analysis of the target mRNA can be achieved. This platform offers significant advantages. First, the high specificity of Cas13 ensures precise recognition of the target mRNA, avoiding interference from nonspecific signals.[27] Second, the nonspecific cleavage activity of Cas13 provides signal amplification, significantly enhancing detection sensitivity.[28] Additionally, the rapid response and portability of the electrochemical biosensor make this platform suitable for on-site testing and point-of-care testing (POCT).[29]

2. Experiment section

2.1 Materials and reagents

Normal intestinal epithelial cells (NCM460) and colorectal cancer cells (DLD-1) were obtained from Prof. Chaoxia Zhou at department of biochemistry and molecular biology, Harbin Medical University (HMU). The DMEM culture medium required for cell culture was obtained from Thermo Fisher-Gibco™, fetal bovine serum was obtained from Clark Bioscience (Virginia, United States), and penicillin/streptomycin was obtained from Beyotime (Shanghai, China). Cas13a and 10× NEBuffer were obtained from Novoprotein (Suzhou, China). HPLC-purified crRNAs, RNase inhibitors, and RNA Markers were obtained from Sangon Biotech Co, Ltd (Shanghai, China). RNase-free water was obtained from Solarbio Science (Beijing, China). 6-Mercapto-1-hexanol (MCH), tris(2-carboxyethyl) phosphine hydrochloride (TCEP), and polyethylene glycol sorbitan monolaurate (Tween-20) were purchased from Aladdin (Shanghai, China). All RNA oligonucleotides were synthesized and purified from Sangon Biotech Co, Ltd (Shanghai, China). All chemicals were used without any further purification and were prepared by dilution with ultrapure water. Unless otherwise stated, all experiments were carried out at room temperature (25 °C).

2.2 Instrumentation

Electrochemical measurements were conducted using the CHI660E electrochemical workstation from Shanghai Chenhua Instrument Co, Ltd. The gel electrophoresis experiment was conducted with DYY-10C electrophoresis apparatus (China Liuyi Instrument Company). Imaging using Azure c300 chemiluminescence imaging system from Azure Biosystems. Atomic force microscopy (Suzhou Feishman Precision Instrument Company) is used to characterize AuNPs on electrode surfaces.

2.3 Configuration probe

The synthesized ReRNA-MB was delivered in lyophilized powder form. Upon receipt, the sample was centrifuged at 5000 rpm for 1 minute, followed by the addition of an appropriate volume of DEPC-treated water to achieve the desired concentration. The solution was then thoroughly mixed using a vortex mixer and briefly centrifuged. After allowing it to stand at 4 °C for 16 hours, the prepared ReDNA-MB was stored at 4 °C for short-term frequent use or at −20 °C for long-term storage.

For further preparation, 5 μL of 1 mmol L^{-1} TCEP (tris(2-carboxyethyl)phosphine) was mixed with 20 μL of thiol-modified ReRNA-MB (10 μmol L^{-1}) and incubated at room temperature for 30 minutes to reduce disulfide bonds. Subsequently, the two prepared reporter probes were heated at 95 °C for 5 minutes and then gradually cooled to room temperature to facilitate the formation of stable hairpin structures through annealing.

2.4 Preparation of the ReRNA-Modified biosensing electrode

Electrochemical measurements were performed using a CHI660E electrochemical analyzer and a three-electrode system, with a platinum wire as the counter electrode, a saturated calomel electrode (SCE) as the reference electrode, and a gold electrode as the working electrode. Cyclic voltammetry (CV) at −0.2–0.6 V was obtained in a 0.5 mM $[Fe(CN)_6]^{3-/4-}$ solution containing 0.1 M KCl, and differential pulse voltammetry (DPV) was obtained in a PBS solution.

The bare GE was freshly polished by using 0.05 μm alumina powder to obtain mirror-like smoothness followed by sonicating with ethanol and deionized water in an ultrasonic bath. The electrode was then immersed into piranha solution (H_2SO_4/H_2O_2 = 3 : 1) for 30 min to remove the residue and washed thoroughly with deionized water. Then, electroplating was carried out in a 1% $AuCl_4$ solution at a voltage of −0.8 V for 100 seconds. After allowing the electrode to air-dry naturally, 8 μL of ReRNA-MB were separately applied to the electrode surface, followed by incubation at 4 °C for 16 hours. Following this, the electrode was immersed into 6 μL of 1 mM MCH solution for 30 min to block the nonspecific sites and obtain a well-aligned DNA monolayer. Finally, after being thoroughly rinsed with the washing buffer, the electrode was allowed to be used for the following operation.

2.5 Cell culture and RNA extraction

(1) After discarding the culture medium, the cells were washed twice with PBS and then digested with 1 mL of trypsin for 3 minutes. The suspension status of the cells was observed under a microscope. Subsequently, 2 mL of culture medium was added to resuspend the cells, and the mixture was transferred to a 15 mL centrifuge tube, followed by centrifugation at 15 000 rpm for 5 minutes. Finally, the supernatant was discarded, and the cells were resuspended in 2 mL of fresh culture medium before being transferred to a new culture flask.

(2) After discarding the culture medium, 1 mL of PBS was added to each well for washing. This washing step was repeated twice, followed by the addition of 1 mL of Trizol to each well for homogenization. The mixture was then transferred to a 1.5 mL EP tube and allowed to stand at room temperature for 5 minutes. Subsequently, 200 μL of chloroform was added to each tube, vortexed until the solution turned pink, and left to stand for another 5 minutes. The samples were then centrifuged at 13 000 rpm for 10 minutes at 4 °C. After centrifugation, 400 μL of the clear supernatant was carefully transferred to a new EP tube, mixed with 400 μL of isopropanol by gentle inversion, and allowed to stand for 10 minutes before being centrifuged for another 10 minutes. The supernatant was discarded, and the pellet was washed twice with 1 mL of 75% ethanol, followed by centrifugation for 5 minutes each time. After air-drying to remove residual ethanol, the RNA pellet was finally dissolved in RNase-free water.

2.6 Target RNA detection protocol

Before the testing, the modified biosensing platform was further rinsed with the washing buffer. Subsequently, the Cas13a-mediated cleavage assay was carried out by adding 10 μL of mixture solution (1 μL 50 nM Cas13a, 1 μL 1 μM crRNA,2 μL 10× NEBuffer, and 1 μL of target RNA) and incubated for 10 min at room temperature. Afterward, the solution was dropped onto the biosensor surface and incubated at 37 °C for 30 min and washed with the washing buffer. The electrochemical differential pulse voltammetry (DPV) measurements were performed in 4 mL of 10 mM PBS (pH 7.4) containing 0.5 M NaCl and 5 mM $MgCl_2$ with a modulation time of 0.05 s, an interval time of 0.017 s, a step potential of 5 mV, a modulation amplitude of 50 mV, and a potential scan from −0.5 to 0.0 V.

2.7 Gel electrophoresis analysis

Prepare a 3% agarose gel to verify the ssRNA enzyme activity of Cas13a. Perform electrophoresis in 0.5× TBE buffer (2 mM EDTA and 89 mM Tris-borate, pH 8.3) at a constant voltage of 100 V for 30 minutes. Finally, visualize the gel using a gel imaging system.

3. Results and discussion

3.1 Sample acquisition and design of Cas13a-electrochemical biosensing system

The specific procedure is illustrated in Fig. 1. Fig. 1A showed the sample detection process, where total RNA was extracted from normal intestinal epithelial cells and intestinal cancer cells using the Trizol method, followed by its addition to the CRISPR–Cas13a reaction system. Upon target-RNA recognition, Cas13a unleashes potent *trans*-cleavage activity that indiscriminately scissions the electrode-anchored hairpin RNA probes tagged with methylene blue (MB). Probe detachment strips the surface of redox reporters, precipitating a sharp drop in faradaic current whose amplitude scales linearly with the target-RNA concentration. This mechanism translates minute quantities of analyte into pronounced electrochemical signals, affording exceptional sensitivity in biosensing applications. Fig. 1B illustrates the electrode preparation process, in which gold nanoparticles (AuNPs) were ated on the GE surface *via* electrodeposition. The spherical AuNPs increased the specific surface area of the electrode, which facilitated the binding of thiol-modified reporter probes to the electrode surface. Subsequently, thiol-modified hairpin reporter probes with the electrochemical label methylene blue (MB) were attached to the electrode surface through Au–S bonds.[30,31] Mercaptohexanol (MCH) was used as a blocking agent to bind any remaining non-specific sites on the surface. After the biosensor was prepared, the solution obtained from Fig. 1A was dropped onto the

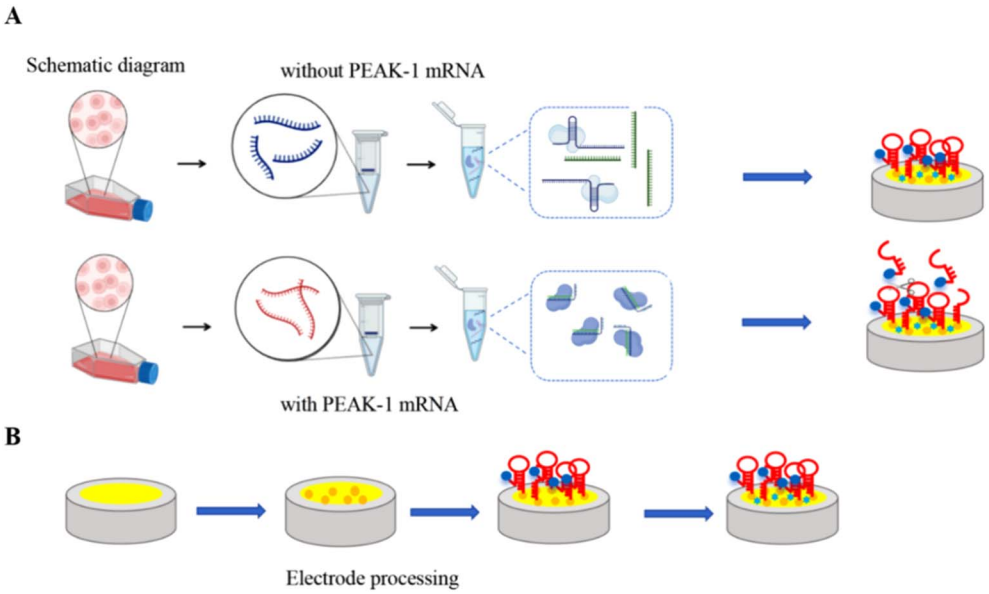

Fig. 1 (A) Sample acquisition and detection; (B) design of Cas13a-electrochemical biosensing system.

electrode surface and incubated at 37 °C for 30 minutes. The preparation process of the biosensor was monitored using differential pulse voltammetry (DPV) and electrochemical impedance spectroscopy (EIS), ensuring the successful implementation of our approach.

3.2 AFM characterization of AuNPs on electrode surface and verification of Cas13a mediated sensing interface cleavage activity

Atomic force microscopy (AFM) is a high-resolution, label-free tool for revealing the three-dimensional topography of electrode surfaces. In this study, AFM was used to track the evolution of the electrode surface after gold plating and the introduction of hairpin probes. The scanning image in Fig. 2A clearly shows significant height contrast, confirming that the hairpin probes have been successfully anchored to the gold electrode surface. The three-dimensional reconstruction in Fig. 2B further displays the stereo conformation of the hairpin probes. Quantitative analysis (Fig. 2C) indicates that the gold plating process increases the surface roughness to 15.3 nm, and the overall height increases to approximately 38.15 nm after the introduction of the probes. The details of the modification process are shown on line 1 of page 2 of the supplementary information.

To verify the cleavage activity mediated by Cas13a on the sensing interface, we used 3% agarose gel electrophoresis to detect different reaction products. As shown in Fig. 2D, in the presence of target RNA, the ReRNA can be specifically recognized and cleaved by the Cas13a–crRNA complex. Lane 1 is ReRNA, lane 2 is the target gene, lane 3 has no target gene but includes the probe and Cas system, and lane 4 is the Cas13a–crRNA-target RNA ternary complex. Comparing lanes 3 and 4, it is evident that in the presence of Cas13a and target RNA, the reporter probe is successfully cleaved. Fig. 2E is the grayscale value statistics of Fig. 2D.

3.3 Electrochemical signal amplification strategy validation and electrochemical characterization of the biosensor

To systematically investigate the differences in the *trans*-cleavage activity of Cas13a towards hairpin ReRNA and linear RNA on the electrode surface, differential pulse voltammetry (DPV) was used to compare their electrochemical responses in parallel under exactly the same experimental conditions, with the detection principle shown in Fig. 3A. When the probes are immobilized on the electrode surface in a linear configuration, methylene blue (MB) is far from the electrode, and electron transfer is hindered, resulting in weak signals. In contrast, when the probes fold into a hairpin structure, MB is brought closer to the electrode surface, significantly enhancing the efficiency of electron coupling and greatly strengthening the signals. As shown in Fig. 3B and C, in the system coexisting with target RNA and the Cas13–crRNA complex, the peak current change (ΔI) of the hairpin ReRNA reporter probe is approximately 1.93 μA. However, when linear RNA was used as the assembled reporter, the initial background peak current was significantly lower, and the subsequent peak current after cleavage remained notable. The ΔI% obtained from the linear RNA reporter was only about 1.36 μA, similar to established results and significantly lower than that of the hairpin ReRNA. The higher initial background peak current of the hairpin ReRNA is attributed to its higher electron transfer rate constant and the closer proximity of the redox label to the electrode surface compared to the linear RNA reporter. Additionally, due to its distinct interfacial properties, the activated Cas13a, oriented toward the exposed loop region of the ReRNA on the surface, demonstrated exceptionally high cleavage efficiency.

To confirm the feasibility and ensure the performance of the electrochemical aptamer biosensor, the biosensor was characterized using cyclic voltammetry (CV) and differential pulse voltammetry (DPV), with the results shown in Fig. 3D and E. Thiolated ReRNA-MB was self-assembled onto the surface of the

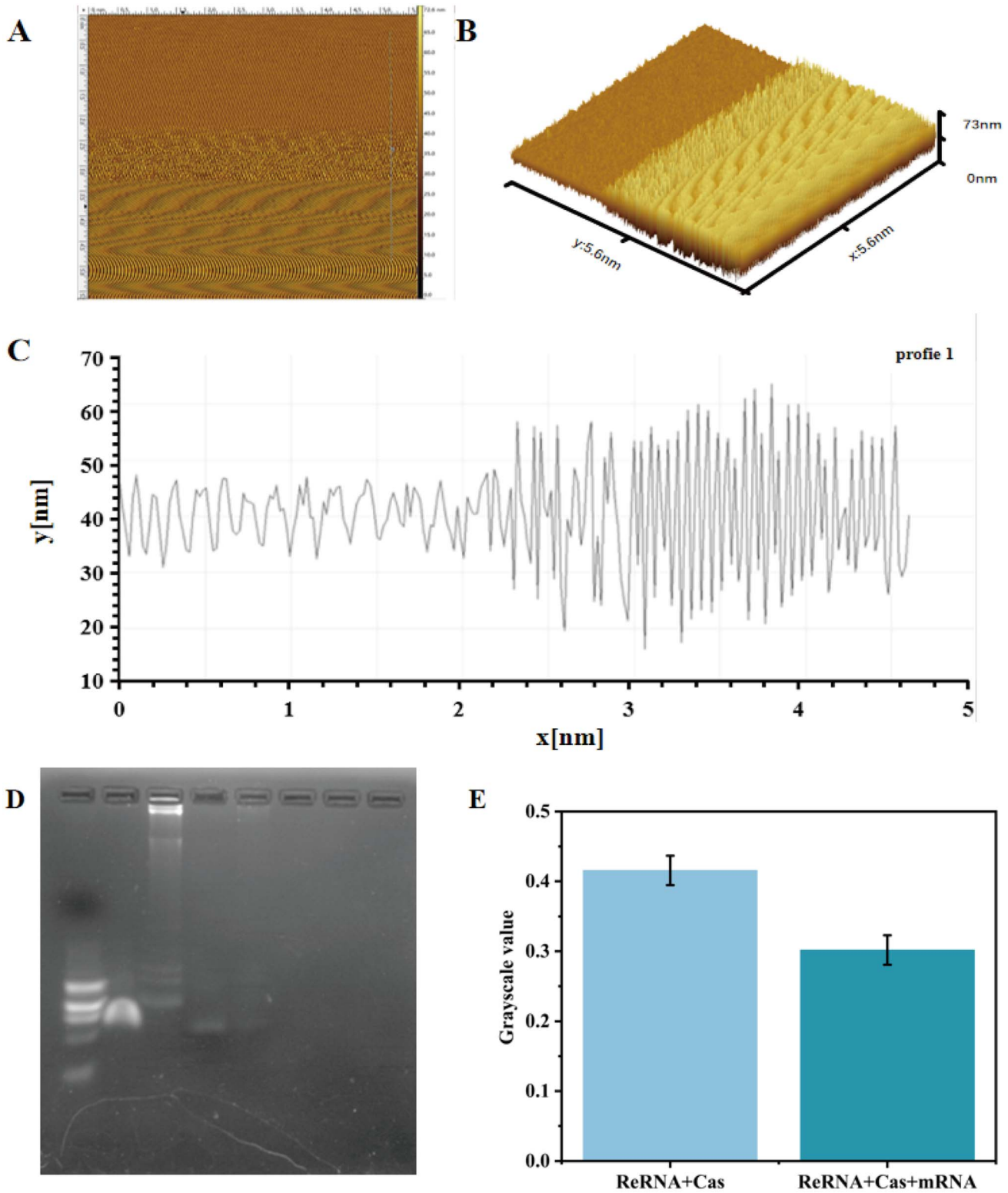

Fig. 2 Characterization of AuNPs (A) AFM scan image; (B) AFM three-dimensional image; (C) AFM cross-sectional height map; (D) agarose gel electrophoresis for the verification of CRISPR/Cas cleavage products; (E) grayscale value statistics of agarose gel electrophoresis bands. (Error bars represent the standard deviation of three independent measurements.)

gold electrode after electroplating *via* Au–S bonds. Due to the hindrance of electron transfer, the CV current decreased. Simultaneously, the peak current of MB, which serves as an electrochemical reporter, could be detected at −0.35 V (blue). After immobilizing MCH on the gold electrode surface, the CV and DPV currents further decreased (green) due to the

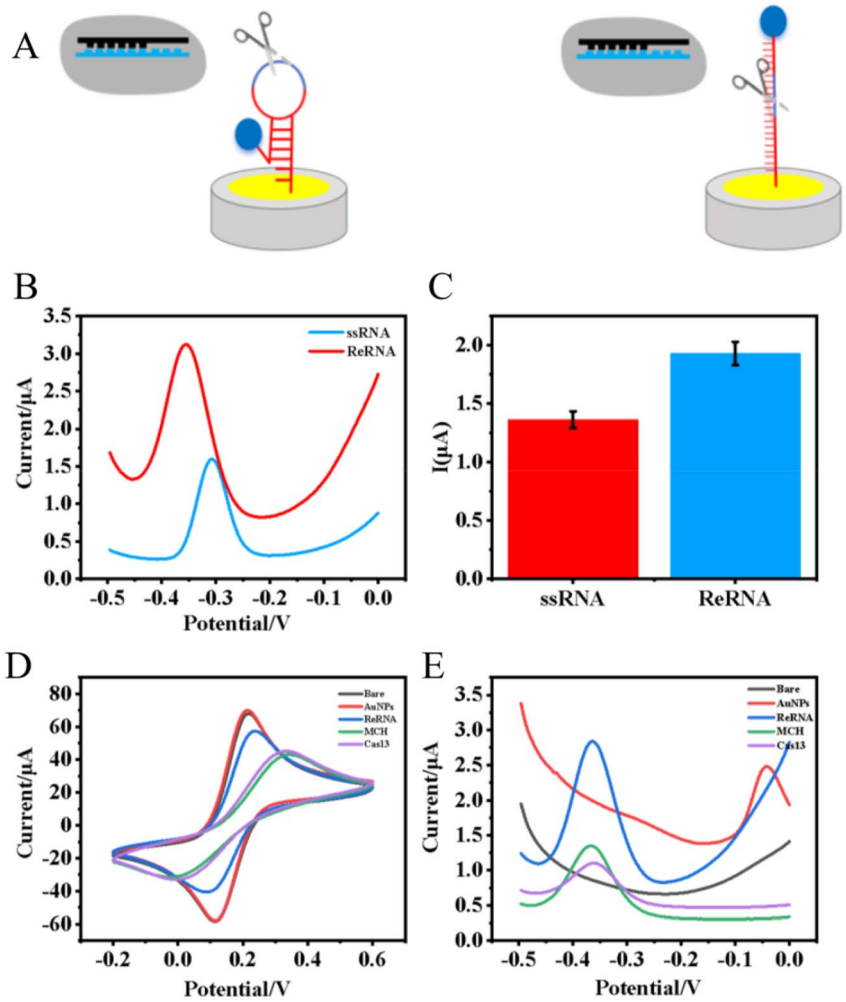

Fig. 3 (A) Schematic diagram of detection principles for linear probes and hairpin probes; (B) DPV curves of ReRNA and ssRNA as reporter probes; (C) peak current statistics chart for ReRNA and ssRNA; (D) the construction process of the biosensing interface was detected using cyclic voltammetry in a solution containing 0.1 M KCl and 5 mM $[Fe(CN)_6]^{3-/4-}$; (E) the construction process of the biosensing interface was detected using differential pulse voltammetry in a PBS solution at pH 7. Bare gold electrode (black), gold-plated (red), hpRNA immobilization (blue), MCH blocking (green), and addition of Cas 13a-crRNA-target RNA ternary complex (purple). (Error bars represent the standard deviation of three independent measurements.)

additional hindrance of electron transfer. Finally, upon the addition of the Cas13–crRNA-target RNA ternary complex, the activated *cis*-cleavage activity also triggered the *trans*-cleavage activity. The nonspecific ReRNA-MB on the electrode surface was digested by the Cas13–crRNA-target RNA ternary complex, shortening the ReRNA on the electrode surface and reducing the hindrance to electron transfer, resulting in an increase in the CV current. Meanwhile, the detachment of MB from the electrode surface led to a decrease in the DPV peak current (purple). Both CV and DPV data confirmed the successful construction of the electrochemical CRISPR/Cas sensing platform.

3.4 Optimization of detection conditions for an electrochemical CRISPR/Cas sensing platform

The DPV detection method was used to optimize the experimental conditions to achieve the best analytical performance. First, the effect of ReRNA immobilization density was investigated. As shown in Fig. 4A and B, the peak current tended to stabilize as the concentration increased from 10 μM to 50 μM. Therefore, 10 μM ReRNA was selected as the optimal concentration for subsequent experiments. Fig. 4C shows the optimization results for the amount of Cas13a enzyme required in the CRISPR reaction system. It can be observed that 1 μL of Cas13a provided the optimal enzymatic activity. Fig. 4D illustrates the optimization of the Cas13a enzyme reaction time. The change in current increased with the extension of the cleavage reaction time, indicating that the *trans*-cleavage mechanism is a continuous process, and the amount of ReRNA cleavage is time-dependent. Considering the time efficiency of the method, 30 minutes was chosen as the appropriate reaction time.

3.5 Electrochemical CRISPR/Cas sensing platform performance evaluation

To ensure the biosensor's capability for effective detection of target mRNA, the dynamic detection range and sensitivity of the

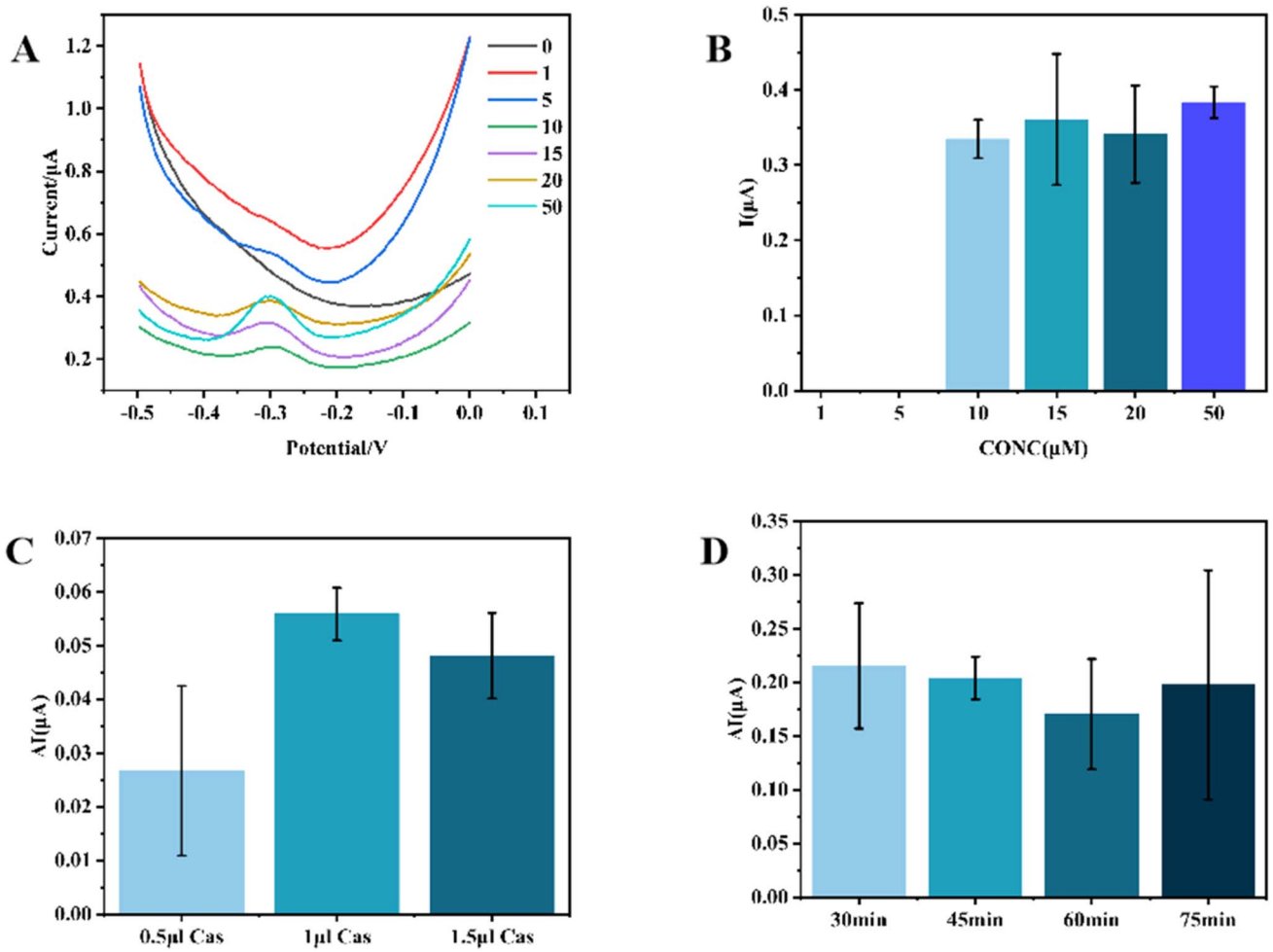

Fig. 4 (A) and (B)The effect of ReRNA concentration on electrochemical signal; (C) and (D) are the effects of Cas enzyme content and reaction time on electrochemical signal, respectively. (Error bars represent the standard deviation of three independent measurements.)

electrochemical CRISPR sensing platform were evaluated under optimal experimental conditions. As shown in Fig. 5, the sensing platform was used to detect samples containing varying concentrations of target mRNA, and the DPV peak current changes increased with the rising concentration of target mRNA. Within the dynamic range of 1 pg μL^{-1} to 10 ng μL^{-1}, the DPV response exhibited a strong linear relationship with the logarithm of the target mRNA concentration. The correlation equation was $Y = 0.23521 + 0.13448\ \lg(C)$, with a correlation coefficient (R^2) of 0.98, where C represents the concentration of target mRNA. Based on the average value of the blank signal and three times the standard deviation, the limit of detection (LOD) was calculated to be 0.45 pg μL^{-1}. As shown in Table 1, our biosensor exhibits excellent performance.[32,33]

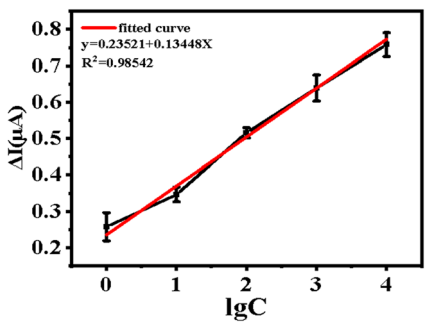

Fig. 5 Calibration curve corresponding to different target mRNA concentrations. (Error bars represent the standard deviation of three independent measurements.)

3.6 Stability and reproducibility of electrochemical CRISPR/Cas sensing platforms

We evaluated the prepared biosensor over seven consecutive days to investigate the stability of our proposed electrochemical biosensor. The biosensors were prepared under optimal conditions, with three biosensors pretreated under these conditions. Three pretreated biosensors were not incubated with target mRNA and were directly subjected to DPV detection. After each measurement, the biosensors were stored at 4 °C. As shown in Fig. 6A, the change was less than 25% during the first seven days of storage. After seven days, it retained 76.05% of the

Table 1 Comparison of biosensor performance

Ref.	Sensing strategy	Target	Detection method	LOD (pg μL^{-1})	Linear range (pg μL^{-1})
Zhang *et al.*[32]	Cas12a-SS DNA	SARS-CoV-2 delta spike RNA	Electrochemical (SWV)	18.9	1–10^4
Lee *et al.*[33]	Cas9	HPV-16 DNA + HPV-18 DNA	Electrochemical (LSV)	013/0.16	1–10^4
Our work	Cas13a-HP RNA	PEAK1 mRNA	Electrochemical (DPV)	0.45	1–10^4

initial current response, indicating that the proposed DNA biosensor exhibits excellent stability.

We tested five electrochemical biosensors at three concentrations (1 μg μL^{-1}, 50 ng μL^{-1}, and 1 ng μL^{-1}) to evaluate the reproducibility among different electrodes. Five independent biosensors were created by modifying five GE electrodes with 1% $HAuCl_4$ solution, hairpin ReRNA, and MCH, respectively. Subsequently, these five biosensors were used to detect the target mRNA at the selected three concentrations. Fig. 6B shows the bar graph of the DPV peak currents obtained from the five biosensors for detecting the target mRNA at the three concentrations. As can be seen from the figure, the differences in the DPV peak currents among the five biosensors were relatively small. The relative standard deviations (RSDs) of the current response values for the five biosensors were calculated to be 6.9% at 1 μg μL^{-1}, 14.2% at 50 ng μL^{-1}, and 6.4% at 1 ng μL^{-1}. This observation demonstrates good reproducibility within an acceptable range, highlighting the consistency and accuracy of the method.

As shown in Fig. 6C, we used a random sequence and PEAK1 protein as negative controls, both with a detection concentration of 1000 ng μL^{-1}, which is 100 times the concentration of the target gene. Neither group produced a significant signal, which fully validated the high specificity of the PEAK1 detection system. To ensure the reliability of a single test, Fig. 6D further evaluated the signal uniformity of the biosensor: 10 sets of peak currents were randomly collected, and the coefficient of variation (CV) was only 1.44%, indicating excellent repeatability. The above results collectively demonstrate that the self-calibrated PEAK1 biosensor can output stable and reliable electrochemical signals, suitable for the precise quantitative analysis of PEAK1.

3.7 Detection specificity of electrochemical CRISPR/Cas sensing platforms

The detection specificity of the electrochemical CRISPR/Cas sensing platform is of paramount importance. To evaluate its specificity, we detected PEAK1 mRNA in two different types of

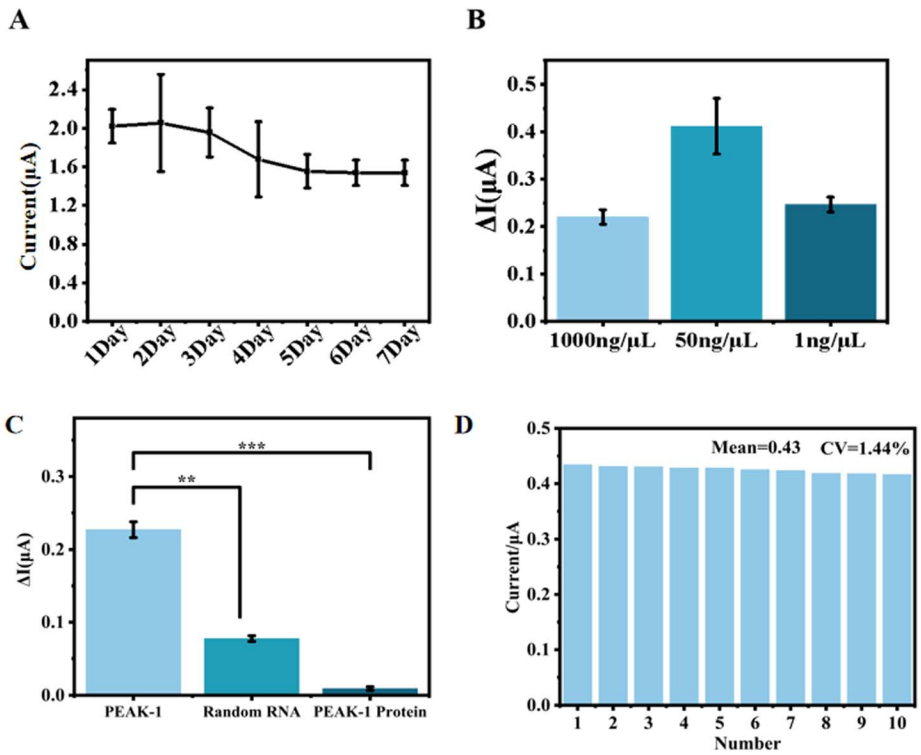

Fig. 6 Stability and reproducibility of the electrochemical CRISPR/Cas sensing platform (A) stability of the biosensor; (B) reproducibility of the biosensor; (C) target gene and random sequences and PEAK1 protein for detection; (D) the signal uniformity of the biosensor. (Error bars represent the standard deviation of three independent measurements, *p < 0.05, **p < 0.01, ***p < 0.001.)

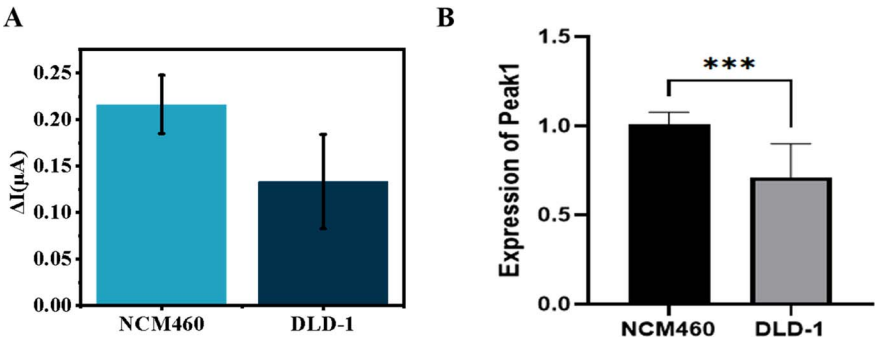

Fig. 7 Detection specificity of the electrochemical CRISPR/Cas sensing platform (A) electrochemical detection results; (B) qPCR results. (Error bars represent the standard deviation of three independent measurements.)

intestinal cells: normal intestinal epithelial cells (NCM460) and colorectal cancer cells (DLD-1). The results are shown in Fig. 7A. Compared to DLD-1, NCM460 exhibited the highest DPV signal difference. Furthermore, we compared the results obtained from the constructed biosensor with those from the gold standard qPCR. As shown in Fig. 7B, the qPCR results were consistent with those detected by our CRISPR–Cas13a-based electrochemical biosensor.

4. Conclusion

PEAK1 promotes cancer cell invasion and metastasis by regulating cytoskeletal dynamics and cell migration, and is closely associated with the progression of various cancers, such as breast cancer and colorectal cancer. Additionally, PEAK1 integrates growth factor signaling (*e.g.*, EGFR, TGF-β) to activate downstream oncogenic pathways, supporting tumor cell proliferation and survival. Its aberrant expression makes it a potential therapeutic target for cancer. Since PEAK1 exhibits abnormal expression in the early stages of cancer, its detection can provide critical insights for early cancer diagnosis. Therefore, the development of highly sensitive methods for PEAK1 detection is of great significance for early cancer screening and precision therapy. In this study, a novel electrochemical biosensor platform was established based on Cas13a-mediated interfacial cleavage of ReRNA-MB for rapid and sensitive nucleic acid detection. The use of hairpin ReRNA enabled higher current signal values, while the incorporation of AuNPs increased the specific surface area, allowing more ReRNA to bind to the electrode surface. The biosensor developed in this study exhibited a broader linear detection range (1 pg μL^{-1} to 10 ng μL^{-1}) and a lower detection limit (0.45 pg μL^{-1}). Additionally, the biosensor demonstrated high stability, reproducibility, and specificity. Compared with the gold standard qPCR, the biosensor we constructed demonstrated high practical utility.

Author contributions

Conceptualization, Xiwei Zhuang, Zhihao Duan and Xue Ge; Data curation, Feiyun Cui; Funding acquisition, Feiyun Cui and Qin Zhou; Methodology, Jianlei Liu, Yuan Gao and Shaoxiong Zhou; Project administration, Qin Zhou; Resources, Jianlei Liu, Shaoxiong Zhou, Chijia Zeng and Feiyun Cui; Supervision, Qin Zhou Feiyun Cui and Chijia Zeng; Validation, Xiwei Zhuang, Xue Ge and Zhihao Duan; Writing – original draft, Xiwei Zhuang, Xue Ge and Zhihao Duan; Writing – review & editing, Feiyun Cui, Yanling Wang and Yuan Gao.

Conflicts of interest

There are no conflicts to declare.

Data availability

The data supporting this article have been included as part of the SI. Supplementary information: the NCBI reference sequence of the Peak1 gene, crRNA sequence, probe sequence, predicted probe structure and atomic force microscopy characterization images of the electrode surface modification process. See DOI: **https://doi.org/10.1039/d5ra05024c**.

Acknowledgements

The work was supported by the National Natural Science Foundation of China (82030065 to Qin Zhou, 82572678 to Feiyun Cui), "Spring Goose" Talent Team Support Program of Heilongjiang Province (2022CYCX0202), Natural Science Foundation of Heilongjiang Province (Excellent Young Scholars Program, JJ2024YX0560), Funding Program for Preferential Returned Scholars of Heilongjiang Province (21032240006), Young Elite Scientist Sponsorship Program of Heilongjiang Province (20240NTJ018). We thanked Biorender (**https://www.biorender.com/**) for their high-quality artwork. We thanked Grammarly (**https://app.grammarly.com/**) for correction of grammatical errors and improvements to readability.

References

1 H. Wang, J. Lapek, K. Fujimura, J. Strnadel, B. Liu, D. J. Gonzalez, W. Zhang, F. Watson, V. Yu, C. Liu, C. M. Melo, Y. I. Miller, K. C. Elliott, D. A. Cheresh and R. L. Klemke, Pseudopodium-Enriched Atypical Kinase 1

Mediates Angiogenesis by Modulating Gata2-Dependent Vegfr2 Transcription, *Cell Discovery*, 2018, **4**, 26.
2 C. Ding, W. Tang, H. Wu, X. Fan, J. Luo, J. Feng, K. Wen and G. Wu, The Peak1-Ppp1r12b Axis Inhibits Tumor Growth and Metastasis by Regulating Grb2/Pi3k/Akt Signalling in Colorectal Cancer, *Cancer Lett.*, 2019, **442**, 383–395.
3 J. Zhu, F. Wang, Y. Weng and J. Zhao, Exosome-Delivered Circsatb2 Targets the Mir-330-5p/Peak1 Axis to Regulate Proliferation, Migration and Invasion of Lung Cancer Cells, *Thorac. Cancer*, 2022, **13**(21), 3007–3017.
4 M. Pan, X. Yin and Y. C. Huang, Pseudopodium Enriched Atypical Kinase 1(Peak1) Promotes Invasion and of Melanoma Cells by Activating Jak/Stat3 Signals, *Bioengineered*, 2021, **12**(1), 5045–5055.
5 J. Strnadel, S. Choi, K. Fujimura, H. Wang, W. Zhang, M. Wyse, T. Wright, E. Gross, C. Peinado, H. W. Park, J. Bui, J. Kelber, M. Bouvet, K. L. Guan and R. L. Klemke, Eif5a-Peak1 Signaling Regulates Yap1/Taz Protein Expression and Pancreatic Cancer Cell Growth, *Cancer Res.*, 2017, **77**(8), 1997–2007.
6 F. Runa, Y. Adamian and J. A. Kelber, Ascending the Peak1 toward Targeting Tgfβ During Cancer Progression: Recent Advances and Future Perspectives, *Cancer Cell Microenviron.*, 2016, **3**(1), e1162.
7 J. A. Kelber and R. L. Klemke, Peak1, a Novel Kinase Target in the Fight against Cancer, *Oncotarget*, 2010, **1**(3), 219–223.
8 H. Gingold and Y. Pilpel, Determinants of Translation Efficiency and Accuracy, *Mol. Syst. Biol.*, 2011, **7**, 481.
9 D. Musaev, M. Abdelmessih, C. E. Vejnar, V. Yartseva, L. A. Weiss, E. C. Strayer, C. M. Takacs and A. J. Giraldez, Upf1 Regulates Mrna Stability by Sensing Poorly Translated Coding Sequences, *Cell Rep.*, 2024, **43**(4), 114074.
10 X. Rambout and L. E. Maquat, Nuclear Mrna Decay: Regulatory Networks That Control Gene Expression, *Nat. Rev. Genet.*, 2024, **25**(10), 679–697.
11 D. Ginsburg, B. A. Konkle, J. C. Gill, R. R. Montgomery, P. L. Bockenstedt, T. A. Johnson and A. Y. Yang, Molecular Basis of Human Von Willebrand Disease: Analysis of Platelet Von Willebrand Factor Mrna, *Proc. Natl. Acad. Sci. U. S. A.*, 1989, **86**(10), 3723–3727.
12 S. Pandey, S. S. McCoy, T. Stobdan and D. Sahoo, Quantitative Mrna Expression Measurement at Home, *Sci. Rep.*, 2024, **14**(1), 1013.
13 J. S. Park, J. Hu, L. Chen and T. H. Wang, Flexpcr: A Streamlined Multiplexed Digital Mrna Quantification Platform with Universal Primers and Limited Fluorescence Channels, *Biosens. Bioelectron.*, 2025, **277**, 117277.
14 Y. Jia, H. Wang, H. Wang, F. Wang, K. Gao and Z. Li, Specific Multiplexed Detection of Mrna Splice Variants Based on Size-Coding DNA Probes and Universal Pcr Amplification, *Analyst*, 2023, **148**(14), 3341–3346.
15 R. Liu, Y. Zhang, M. Liu, Y. Ni, Y. Yue, S. Wu and S. Li, Electrochemical Sensor Based on Fe(3)O(4)/A-Fe(2)O(3) @Au Magnetic Nanocomposites for Sensitive Determination of the Tp53 Gene, *Bioelectrochemistry*, 2023, **152**, 108429.
16 M. Li, L. Wang, Y. Hu, Y. Liu, S. Xu, K. Peng, C. Li, H. Huang, L. Fang, L. Li, H. Liu, X. Wang and J. Zheng, A Strategy for Electrochemical Biosensing Based on Dendritic Hcr Amplification for Detection of Rna M5c and M6a Methylation, *Anal. Chim. Acta*, 2025, **1347**, 343796.
17 S. Noreen, I. Ishaq, M. H. Saleem, B. Ali, S. Muhammad Ali and J. Iqbal, Electrochemical Biosensing in Oncology: A Review Advancements and Prospects for Cancer Diagnosis, *Cancer Biol. Ther.*, 2025, **26**(1), 2475581.
18 P. Chandra, Affordable and Sustainable Biosensing Technology, *Nanotheranostics*, 2025, **9**(1), 63–66.
19 Y. Zhang, S. Li, R. Li, X. Qiu, T. Fan, B. Wang, B. Zhang and L. Zhang, Advances in Application of Crispr-Cas13a System, *Front. Cell. Infect. Microbiol.*, 2024, **14**, 1291557.
20 M. J. Kellner, J. G. Koob, J. S. Gootenberg, O. O. Abudayyeh and F. Zhang, Sherlock: Nucleic Acid Detection with Crispr Nucleases, *Nat. Protoc.*, 2019, **14**(10), 2986–3012.
21 O. O. Abudayyeh, J. S. Gootenberg, P. Essletzbichler, S. Han, J. Joung, J. J. Belanto, V. Verdine, D. B. T. Cox, M. J. Kellner, A. Regev, E. S. Lander, D. F. Voytas, A. Y. Ting and F. Zhang, Rna Targeting with Crispr-Cas13, *Nature*, 2017, **550**(7675), 280–284.
22 P. Shi and X. Wu, Programmable Rna Targeting with Crispr-Cas13, *RNA biology*, 2024, **21**(1), 1–9.
23 J. S. Gootenberg, O. O. Abudayyeh, J. W. Lee, P. Essletzbichler, A. J. Dy, J. Joung, V. Verdine, N. Donghia, N. M. Daringer, C. A. Freije, C. Myhrvold, R. P. Bhattacharyya, J. Livny, A. Regev, E. V. Koonin, D. T. Hung, P. C. Sabeti, J. J. Collins and F. Zhang, Nucleic Acid Detection with Crispr-Cas13a/C2c2, *Science*, 2017, **356**(6336), 438–442.
24 G. Zhu, X. Zhou, M. Wen, J. Qiao, G. Li and Y. Yao, Crispr-Cas13: Pioneering Rna Editing for Nucleic Acid Therapeutics, *BioDesign Res.*, 2024, **6**, 0041.
25 L. Hao, R. T. Zhao, N. L. Welch, E. K. W. Tan, Q. Zhong, N. S. Harzallah, C. Ngambenjawong, H. Ko, H. E. Fleming, P. C. Sabeti and S. N. Bhatia, Crispr-Cas-Amplified Urinary Biomarkers for Multiplexed and Portable Cancer Diagnostics, *Nat. Nanotechnol.*, 2023, **18**(7), 798–807.
26 T. Zhou, R. Huang, M. Huang, J. Shen, Y. Shan and D. Xing, Crispr/Cas13a Powered Portable Electrochemiluminescence Chip for Ultrasensitive and Specific Mirna Detection, *Adv. Sci.*, 2020, **7**(13), 1903661.
27 Y. Wang, Y. Zhang, J. Chen, M. Wang, T. Zhang, W. Luo, Y. Li, Y. Wu, B. Zeng, K. Zhang, R. Deng and W. Li, Detection of Sars-Cov-2 and Its Mutated Variants *Via* Crispr-Cas13-Based Transcription Amplification, *Anal. Chem.*, 2021, **93**(7), 3393–3402.
28 D. Shihong Gao, X. Zhu and B. Lu, Development and Application of Sensitive, Specific, and Rapid Crispr-Cas13-Based Diagnosis, *J. Med. Virol.*, 2021, **93**(7), 4198–4204.
29 W. Heo, K. Lee, S. Park, K. A. Hyun and H. I. Jung, Electrochemical Biosensor for Nucleic Acid Amplification-Free and Sensitive Detection of Severe Acute Respiratory Syndrome Coronavirus 2 (Sars-Cov-2) Rna *Via* Crispr/Cas13a Trans-Cleavage Reaction, *Biosens. Bioelectron.*, 2022, **201**, 113960.

30 D. Zhang, Y. Yan, H. Que, T. Yang, X. Cheng, S. Ding, X. Zhang and W. Cheng, Crispr/Cas12a-Mediated Interfacial Cleaving of Hairpin DNA Reporter for Electrochemical Nucleic Acid Sensing, *ACS Sens.*, 2020, **5**(2), 557–562.

31 Y. Dai, R. A. Somoza, L. Wang, J. F. Welter, Y. Li, A. I. Caplan and C. C. Liu, Exploring the Trans-Cleavage Activity of Crispr-Cas12a (Cpf1) for the Development of a Universal Electrochemical Biosensor, *Angew. Chem., Int. Ed.*, 2019, **58**(48), 17399–17405.

32 C. Wu, Z. Chen, C. Li, *et al.*, CRISPR-Cas12a-Empowered Electrochemical Biosensor for Rapid and Ultrasensitive Detection of SARS-CoV-2 Delta Variant, *Nano-Micro Lett.*, 2022, **14**(1), 159.

33 H. V. Nguyen, S. Hwang, S. W. Lee, E. Jin and M. H. Lee, Detection of HPV 16 and 18 L1 genes by a nucleic acid amplification-free electrochemical biosensor powered by CRISPR/Cas9, *Bioelectrochemistry*, 2025, **162**, 108861.